Investigation of thermally induced Li^+ ion disorder in Li_2O using neutron diffraction

1991 J. Phys.: Condens. Matter 3 4761

(http://iopscience.iop.org/0953-8984/3/26/001)

J. Phys.: Condens. Matter 3 (1991) 4761–4781. Printed in the UK

Investigation of thermally induced Li^+ ion disorder in Li_2O using neutron diffraction

T W D Farley†¶, W Hayes†, S Hull †||, M T Hutchings‡ and M Vrtis§

† Clarendon Laboratory, Parks Road, Oxford OX1 3PU, UK
‡ NDT Department, Harwell Laboratory, Didcot OX11 0RA, UK
§ Institut Laue–Langevin, BP156, 38042 Grenoble, France

Received 14 February 1991

Abstract. Neutron diffraction measurements have been performed on a single crystal of $^7Li_2O$ to investigate the time-averaged positions of the nuclei at seven temperatures between 293 and 1603 K. At temperatures up to 873 K the observed Bragg peak intensities can be well fitted using the regular antifluorite structure, including harmonic and anharmonic temperature factors to describe the thermal vibrations. At higher temperatures an improved fit to the experimental data is obtained by allowing a fraction of cations to leave their regular lattice sites. This is indicative of a transition to a 'fast-ion' phase, analogous to that observed in the fluorite-structured compounds at elevated temperatures. The model of the time-averaged disordered structure which best fits the data consists of interstitial lithium ions occupying mean positions very close to the midpoint between two nearest-neighbour Li^+ ions. The fraction of Li^+ ions occupying these sites increases rapidly above 1200 K, reaching approximately 16% at 1603 K. There is some evidence that the presence of the interstitial cations produces slight relaxations of the two nearest-neighbour Li^+ ions in ⟨111⟩ directions, away from the interstitial.

1. Introduction

Lithium oxide, Li_2O, has the antifluorite crystal structure (space group $Fm\bar{3}m$), in which the Li^+ ions form a simple cubic array, of spacing $a_0/2$ ($a_0 \approx 4.61$ Å at 293 K), and the O^{2-} ions occupy alternate cube centres. Many fluorite-structured compounds such as CaF_2, $SrCl_2$ and UO_2, in which the positions of cations and anions are reversed, undergo a diffuse transition to a 'fast-ion' phase at a temperature well below the melting temperature T_m. This phase is characterized by thermally induced dynamic disorder in the anion sublattice, which can be modelled by short-lived anion Frenkel clusters (Hayes and Hutchings 1989). In analogy, Li_2O might be expected to become a fast-ion conductor at elevated temperatures, with the Li^+ cation being the highly mobile species. This suggestion has been supported by measurements of the self-diffusion coefficients of lithium and oxygen ions in Li_2O by Oishi *et al* (1979) and Akiyama *et al* (1981), respectively.

¶ Present address: Alcan International Ltd, Banbury Laboratory, Southam Road, Banbury OX16 7SP, UK.

|| Present address: ISIS Science Division, ISIS Facility, Rutherford Appleton Laboratory, Didcot OX11 0QX, UK.

0953-8984/91/264761+21$03.50

Li_2O has important technological applications as a leading contender for the role of blanket breeding material in future nuclear fusion reactors (Kulcinski *et al* 1986, Harries *et al* 1985, Johnson *et al* 1988, Smith *et al* 1985). The purpose of the blanket, which surrounds the first wall of the plasma containment vessel, is to convert energetic neutrons into usable heat and to breed the tritium necessary to sustain the D–T fusion reaction. The main advantages of Li_2O lie in its high lithium density, which exceeds that of lithium metal by a factor of about two; high melting temperature (T_m = 1705 K, Liu *et al* 1985); low tritium solubility; high thermal conductivity and reasonably rapid tritium release. However, one potential problem relates to its large coefficient of thermal expansion, leading to possible mechanical interaction between the Li_2O and its surrounding environment. The first accurate determination of the bulk mechanical properties of Li_2O at high temperatures, from which this interaction may be assessed, has been made by Hull *et al* (1988). Ohno *et al* (1985) have established that the behaviour of tritium ions in Li_2O is very similar to that of the lithium ions. Consequently, the study of lithium ion mobility may provide insight into the motion of tritium in the Li_2O lattice. This is the subject of a separate, future publication (Farley *et al* 1990).

Neutron diffraction gives information on the time-averaged positions of nuclei within the unit cell, together with their average thermal motion. If, as in this case, the ordered structure is known, the technique may be used to assess the extent and nature of any disordering of this basic structure. Neutron diffraction has been particularly successful in the study of anion disorder in the fast-ion phase of fluorite compounds, such as PbF_2 (Dickens *et al* 1982, Hayes and Hutchings 1989).

In this paper neutron diffraction measurements made on a single crystal of $^7Li_2O$ at temperatures between 293 and 1603 K are reported. Analysis of the Bragg intensities at each temperature in terms of a number of possible models of the time-averaged disorder has been used to establish the nature of the dynamic cation disorder in the fast-ion phase of this material. A single crystal is used in preference to powder samples to avoid the problems associated with diffraction peak overlap and powder crystallization at high temperatures. Nevertheless, single crystal measurements are subject to large systematic corrections due to several factors, including thermal diffuse scattering (TDS) and extinction. The results are compared with recent calculations of the formation energies of various defects induced at high temperatures in Li_2O (Chadwick *et al* 1988).

2. Experimental procedure

2.1. Sample and diffractometer

The experiment described here used a single crystal of isotopically pure $^7Li_2O$, because of the large thermal neutron absorption coefficient of the ^6Li nucleus. Lithium carbonate (Li_2CO_3) starting material of isotopic purity 99.950 at% ^7Li was obtained from Oak Ridge National Laboratory and reduced to $^7Li_2O$ powder by heating for 48 h at 970 K under high vacuum. The crystal was grown in a Pt crucible using the vertical Bridgman technique by Dr R C C Ward of the Clarendon Laboratory Crystal Growth Group, Oxford. The sample used in the diffraction experiment was cut ultrasonically, parallel to the $[1\bar{1}0]$ crystallographic axis, to form a cylinder of length 5 mm and diameter 1.5 mm. The cut crystal was encapsulated inside a Pt tube with a wall thickness

of approximately 0.1 mm, the ends of which were crimped flat and electron beam welded under vacuum.

The experiment was performed using the 2-circle mode of the single crystal diffractometer, D15, at the ILL, Grenoble. The sample was held by a molybdenum mount and suspended inside a standard ILL neutron beam furnace. The temperature was measured by a W–5%Re/W–26%Re thermocouple positioned just above the sample. Measurements were made at seven different temperatures between 293 and 1603 K with temperature stability better than ±5 K at all temperatures. The majority of measurements were performed using neutrons of wavelength $\lambda = 0.854$ Å.

After stabilizing at each temperature the crystal was carefully adjusted to lie on the instrument axis and in the centre of the beam. Standard alignment routines were used to orientate the crystal and determine the UB matrix, which describe its orientation with respect to the instrument axes. This matrix was used to automatically reorient the sample in order to collect data from between 26 and 34 independent Bragg reflections at each temperature, out to a maximum of $h^2 + k^2 + l^2 = 91$. The intensity of each reflection was obtained by integrating over $\omega - 2\theta$ scans, composed of 29 points. The counting time per point varied from 8 to 66 s, depending on the intensity of the reflection. To enable subtraction of possible background scattering from the sample environment, each reflection scan was repeated with the crystal offset from the Bragg setting by approximately 4°. The lattice parameter, a_0, was determined at each temperature from the alignment procedure. These values of a_0 are summarized, together with previous data, in table 1.

Table 1. Temperature variation of the lattice constant, a_0, of Li_2O. The figures in parentheses indicate the estimated error in the last decimal place. The temperatures marked + indicate values obtained during the diffraction experiment described in this paper. The other values given are those of Hull *et al* (1988) and Farley *et al* (1990).

Temperature (K)	a_0 (Å)
293	4.60(1)
293+	4.610(5)
293+	4.612(5)
523	4.64(1)
773	4.69(1)
873+	4.689(5)
873+	4.693(5)
973	4.71(1)
1123+	4.728(5)
1123	4.73(1)
1273+	4.764(5)
1273	4.77(1)
1373	4.78(1)
1373+	4.782(5)
1473+	4.807(5)
1473	4.81(1)
1603+	4.837(5)
1603	4.85(1)

Two standard reflections, the (002) and (442), were measured at the start, middle and end of each set of scans at temperatures above 873 K. They were used to monitor any changes of intensity with time at elevated temperatures. The strong high-angle

(442) reflection is expected to be mainly affected by crystal loss. Its intensity remained constant with time within error, so that this effect could be neglected. The strong low-angle (002) reflection is, in addition, a good monitor of extinction. This indicated an increase in crystal extinction with time at the highest temperatures as the crystal became more perfect. For this reason the intense low-angle reflections were not included in the subsequent analysis.

2.2. Corrections to the experimental data

In general, corrections to single crystal diffraction data are required for TDS, extinction and absorption. These effects can be expressed as correction factors that modify the expression for the theoretical integrated Bragg intensity, $I_c(hkl)$.

$$I_c(hkl) = A(y+\alpha)S|F_c(hkl)|^2/\sin 2\theta. \tag{1}$$

Here A, y and α are the correction factors for absorption, extinction and TDS respectively. S is the scale factor, which is related to the ratio N/V, where N is the number of unit cells in the sample, which has volume V. $F_c(hkl)$ is the calculated structure factor for the (hkl) reflection. The absorption correction is, in fact, negligible for $^7Li_2O$ because of the small absorption cross section of the ^{7}Li and O nuclei and the small sample size.

The corrections for TDS and extinction are now considered individually.

2.2.1. TDS correction. TDS arises from scattering of neutrons from small wavevector phonons which are detected in a diffraction experiment, along with Bragg scattering, due to the lack of energy analysis in the diffractometer. In general, the contribution from TDS is dominated by acoustic phonons and rises to a maximum at the same position in reciprocal space as the Bragg reflection. It can, therefore, lead to an appreciable error in the measured reflection intensity, particularly at elevated temperatures. The steepness and anisotropic nature of the acoustic branch dispersion surfaces in Li_2O (Hull *et al* 1988) complicate the problem of calculating a correction factor, since the transverse phonon velocities lie in both the faster than sound and slower than sound regimes (Cooper and Rouse 1968, Cooper 1971). The situation has been considered in detail by Farley (1989), where a full account of the factor α at each temperature is given. It was found, however, that they differ only slightly from those calculated using standard faster than sound theory.

Any error in the TDS correction factors can be shown to result only in an error in the thermal parameters B_i, and will not significantly affect the accuracy of other parameters determined from the measured intensities (Willis 1970). It is estimated that in this case the error in the values of α is $\leq 20\%$, which gives rise to a maximum systematic error in the thermal vibration parameters of approximately 2%.

2.2.2. Extinction correction. Extinction arises from the attenuation of the scattered neutron flux by diffraction processes within the crystal. Primary extinction, due to individual mosaic blocks, is usually neglected in real crystals and the correction factor y can be calculated from the theories of secondary extinction. The extinction correction factor used in this analysis is calculated from the theory of Cooper and Rouse (1970), which is an extension of the theory formulated by Zachariasen (1967) to cope with higher levels of extinction (up to 80% reduction in intensity).

The extinction factor, y, is given by

$$y = 1 - 1/f(\theta) + y'/f(\theta) \tag{2}$$

where

$$f(\theta) = 1 + (\sin\theta)^{2.5}/3. \tag{3}$$

For a cylindrical crystal

$$y' = [\sqrt{\pi}/2\,\mathrm{erf}\{\sqrt{(3X(\theta))}\}/\sqrt{(3X(\theta))}]^{5/4} \tag{4}$$

where

$$X(\theta) = |F(hkl)|^2\lambda^2 e/\sin 2\theta \tag{5}$$

and e is an extinction parameter. It is difficult to calculate an absolute extinction correction and thus it is better to fit the parameter e freely to the data at each temperature (Larson 1967).

3. Data analysis

In principle it is possible to obtain a time-averaged picture of the probability density function of nuclei over the unit cell by making a Fourier transform of the complete set of structure factors $F(hkl)$. However, in practice there are problems with this approach arising from termination errors, an incomplete set of structure factors, with possibly some uncertain phase factors, and from systematic errors described in the previous section which are difficult to calculate accurately *a priori*.

A common alternative method of analysis, which has been adopted here, involves the comparison of the measured Bragg intensities, after background and TDS corrections have been made, with calculated intensities derived from models of the time-averaged ionic positions. These models also assign harmonic and anharmonic temperature factors to the ions to describe the effects of thermal vibration. The numbering of the models is close to that used by Dickens *et al* (1982).

3.1. Models of the regular and disordered structure

The simplest model which can be fitted to the data is the defect-free regular anti-fluorite structure. Apart from the extinction correction parameter, e, the only fitted parameters are those relating to the thermal vibrations of each ion, i. Dawson *et al* (1967) have considered these vibrations to be governed by an effective one-particle potential, $V_i(\boldsymbol{r})$, for each ion:

$$V_i(\boldsymbol{r}) = V_{0i} + \alpha_i(x^2 + y^2 + z^2) + \beta_i(xyz) + \text{higher order terms} \tag{6}$$

where the coefficients α_i and β_i describe the harmonic and anharmonic terms in the potential function.

Model I considers only isotropic vibrations of each ion and thus all the terms beyond the second, harmonic term are assumed to be zero. Each ion has an isotropic thermal parameter, B_i, which is related to α_i by

$$B_i = 8\pi^2 k_B T/\alpha_i. \tag{7}$$

B_i is related to the mean-square ionic displacement of the ion i, $\langle u_i^2 \rangle$ by

$$B_i = 8\pi^2 \langle u_i^2 \rangle / 3. \tag{8}$$

Diffraction studies of CaF_2 (Willis 1965), BaF_2 (Cooper and Rouse 1968) and SrF_2 (Forsyth *et al* 1989) have shown that it is necessary to consider anharmonic thermal vibrations of the regular site anions within the fluorite lattice. For the antifluorite Li_2O, this vibrational anisotropy is a consequence of the lack of inversion symmetry at the Li^+ cation site, which leads to a greater average amplitude of thermal vibration of the cation in the directions of the empty cube centre sites. Model Ia therefore includes an anharmonic thermal vibration parameter for the lithium ions, ${}^{AN}B_{Li}$, which is related to the asymmetric cubic term by

$${}^{AN}B_{Li} = 8\pi^3 \beta_{Li} (k_B T)^2 / (a_0 \alpha_{Li})^2 = -C^0_{123} \tag{9}$$

where C^0_{123} is the third-order cumulant coefficient discussed by Willis and Hazell (1980). The oxygen ions are assumed to vibrate isotropically (i.e. have $\beta_O = 0$). All the subsequent models include anisotropic thermal vibrations of the Li^+ ions.

Model II introduces the simplest form of defect into the regular structure by allowing the coherent neutron scattering length of the lithium ions, b_{Li}, to vary to an effective value, b'_{Li}. A reduction in b_{Li} is formally equivalent to a time-averaged fraction of lithium ions, n_d, leaving their regular lattice sites to occupy random interstitial positions within the unit cell, with

$$n_d = 1 - b'_{Li}/b_{Li}. \tag{10}$$

The remaining models are discussed in terms of vacancies on the regular cation sites and the occupation, by the displaced ions, of two types of defective site, labelled 'I' and 'R'. The two sites are illustrated in figure 1 and correspond to $48i$ and $32f$ sites in standard Wykoff notation. Relative to the empty cube centre site, there are 12 I sites, with positional parameter y, at positions $\pm(\frac{1}{4} - y)a_0, \pm(\frac{1}{4} - y)a_0, 0$ etc, and 8 R sites, with positional parameter x, at positions $\pm(\frac{1}{2} - x)a_0$, $\pm(\frac{1}{2} - x)a_0, \pm(\frac{1}{2} - x)a_0$. From figure 1 it can be seen that the I sites are displaced $a_0 y\sqrt{2}$ towards the empty cube centre in a $\langle 110 \rangle$ direction away from the midpoint between two nearest-neighbour regular site cations. The R sites are at distance $a_0 x\sqrt{3}$ from the cation in a $\langle 111 \rangle$ direction towards the empty cube centre. Displaced lithium ions occupying I sites are true Frenkel interstitials, compared with lithium ions occupying R sites which are relaxed away from their regular sites, due to the close proximity of a true interstitial ion. Limiting the analysis to these specific sites is justified on both theoretical and experimental grounds. Past studies of fluorite compounds have shown that both neutron diffraction data and coherent diffuse neutron scattering data can be well accounted for by assuming such models for the disordered structure (Hutchings *et al* 1984). Static energy calculations of the formation energy of defect clusters in the fluorite lattice (Catlow and Hayes 1982) suggest that occupation of I and R sites is energetically favourable for stable, if static, cluster formation.

Models III to VI assume that the displaced lithium ions occupy just one of the two types of site. In model III, the displaced lithium ions are all constrained to occupy the empty cube centre site, defined as an R site with $x = 0.5$. For this model and all subsequent models, except for model IVa, the harmonic thermal vibration

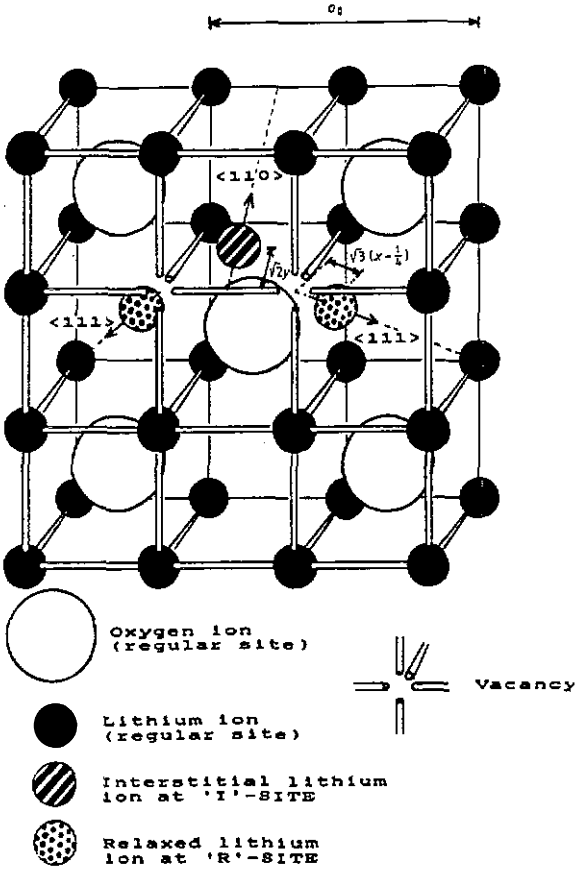

Figure 1. Schematic illustration of I and R sites in the antifluorite lattice of Li_2O.

parameter for a displaced lithium ion, B^{I}_{Li} or B^{R}_{Li}, in its defective site, I or R, is constrained to equal the regular site value, B_{Li}, as the data often do not allow its separate determination. In models IV and IVa the displaced cations are all constrained to occupy a site on the cube-edge, midway between two regular site cations, defined as an I site with $y = 0$. Model IVa differs from model IV by allowing B^{I}_{Li} to vary independently. Model V is an extension of model III, still constraining all the displaced lithium ions to occupy R sites, but allowing x to vary away from an arbitrary starting position of $x = 0.3$. Similarly, model VI is an extension of model IV, allowing y to vary away from the cube-edge position towards the empty cube-centre.

Model VII represents a defect cluster, consisting of both I and R site occupation. The parameter d_x is introduced which defines the fraction of all the displaced cations that are assumed to occupy R sites as opposed to I sites. Hence, the fraction of all cations in the sample that are true Frenkel interstitials, n_f, is given by

$$n_f = n_d(1 - d_x). \tag{11}$$

In model VII, d_x is fixed to value of $\frac{2}{3}$, corresponding to the defect cluster shown in figure 1. This is termed a 3:1:2 cluster, where the notation vacancies:interstitials:relaxed ions is used, and represents the situation where the presence of a Frenkel interstitial on an I site is accompanied by two nearest-neighbour relaxed cations on R sites. Finally,

the most complex model considered is model VIII, which is an extension of model VII which allows d_x to vary.

Consideration of the expressions for the structure factors for each model, listed in appendix 1, shows that the positional parameter x and the anharmonic thermal vibration parameter ${}^{AN}B_{Li}$ are potentially correlated, since both contribute to the differing intensities of reflections with $h + k + l = 2n \pm 1$ which occur at the same scattering angle 2θ. Consequently, if such correlations were apparent, it proved necessary to fix ${}^{AN}B_{Li}$ to values well determined from simpler models that do not involve R sites. A summary of these models, listing the fitted parameters for each, is given in table 2.

Table 2. Summary of the models of the time-averaged structure of Li_2O and their fitted parameters.

Model	Description	Fitted parameters
I	Regular antifluorite (harmonic vibrations)	e, B_{Li}, B_O
Ia	Regular antifluorite (anharmonic vibrations)	$e, B_{Li}, B_O, {}^{AN}B_{Li}$
II	Vacancies only (uniformly distributed defective cations)	$e, B_{Li}, B_O, {}^{AN}B_{Li}, b_{Li}$
III	Cube-centre interstitial (R site with $x = 0.5$; $B_{RLi} = B_{Li}$)	$e, B_{Li}, B_O, {}^{AN}B_{Li}, n_d$
IV	Cube-edge interstitial (I site with $y = 0.0$; $B_{ILi} = B_{Li}$)	$e, B_{Li}, B_O, {}^{AN}B_{Li}, n_d$
IVa	Cube-edge interstitial (I site with $y = 0.0$)	$e, B_{Li}, B_O, {}^{AN}B_{Li}, B_{ILi}, n_d$
V	R site only ($B_{RLi} = B_{Li}$)	$e, B_{Li}, B_O, {}^{AN}B_{Li}, n_d, x$
VI	I site only ($B_{ILi} = B_{Li}$)	$e, B_{Li}, B_O, {}^{AN}B_{Li}, n_d, y$
VII	R and I sites as 3:1:2 cluster ($d_x = 0.67; B_{RLi} = B_{ILi} = B_{Li}$)	$e, B_{Li}, B_O, {}^{AN}B_{Li}, n_d, x, y$
VIII	R + I sites as cluster ($B_{RLi} = B_{ILi} = B_{Li}$)	$e, B_{Li}, B_O, {}^{AN}B_{Li}, n_d, x, y, d_x$

3.2. Least-squares fitting procedure

The various models for the disordered time-averaged structure, described in the previous section, were fitted in turn to the diffraction data at each temperature, using a version of the program POWLS (written by W G Hamilton). This routine uses the method of least-squares refinement to minimize the weighted R-factor, R_w, which is defined by

$$R_w^2 = \sum_i [(I_{oi} - I_{ci})/\Delta I_{oi}]^2 / \sum_i [I_{oi}/\Delta I_{oi}]^2 \qquad (12)$$

I_{oi} and I_{ci} are the observed and calculated values of the ith integrated peak intensity and ΔI_{oi} is the error in the observed intensity. Clearly, R_w does not take into account the number of fitted parameters in the fitted model or the number of data points

included in the fit. Judgment as to whether a better fit was obtained by using a model containing more parameters was made using the significance testing criteria of Hamilton (1965) and by checking the the final fitted values were physically sensible.

The strong Bragg reflections (111), (002) and (222) were not included in the fitted dataset owing to their excessive extinction corrections. The scale factor S in equation (1) was obtained by fitting model Ia to the two datasets at 873 K, measured before and after the high temperature scans, with S as a fitted parameter. At higher temperatures $S(T)$ was kept fixed at a value determined using the average of these two values and the expression

$$S(T) = S(873\ \text{K})[a_0(T)/a_0(873\ \text{K})]^3. \tag{13}$$

Fixing $S(T)$ can be justified on the grounds of reducing the number of fitted parameters in the models, but also because of the strong correlations between the scale factor and the extinction factor, e.

4. Results

The minimum values of R_w obtained for each model are summarized in table 3, together with the model giving the best fit to the observed data at each temperature, after testing for significance (Hamilton 1965). The values of the parameters resulting from the model which best fits the data are given in table 4 at each temperature. A comparison of the observed intensities of the Bragg reflections with those calculated from the best-fitting parameters is given in appendix 2.

Table 3. Values of the minimum weighted R-factor, R_w, obtained by fitting each model of the disordered structure to the n experimental data at each temperature. m is the number of fitted parameters in each model and R_w (min) is the value of R_w for an ideal fit, for which $I_o - I_c = \Delta I_o$. R_w is given in parentheses if one or more fitted parameters have values that are physically unrealistic.

		Temperature (K)							
	m	293	873	873	1123	1273	1373	1473	1603
n		31	23	31	31	23	23	23	27
I	3	4.57	6.69	5.83	7.71	10.61	13.06	15.03	21.51
Ia	4	4.42	3.81	3.57	4.87	5.39	6.82	9.52	14.72
II	5	4.37	3.61	3.49	4.29	4.85	5.94	7.92	10.07
III	5	(4.41)	(3.73)	(3.53)	(4.86)	(5.38)	(6.80)	(9.34)	(14.51)
IV	5	4.41	3.77	3.53	4.45	4.76	5.28	6.64	9.57
IVa	6	—	—	—	—	4.75	4.97	6.17	9.56
V	6	—	—	—	4.23	(4.00)	5.10	(6.15)	9.65
VI	6	4.38	3.79	3.48	4.55	4.16	5.98	8.42	9.55
VII	6	(4.31)	(14.40)	3.44	4.14	4.24	5.27	11.52	9.22
VIII	7	—	—	3.43	4.07	(7.16)	—	—	9.22
R_w (min)		3.40	5.22	3.83	4.31	5.14	5.77	6.13	6.90
Best model		Ia	Ia	Ia	II	VI	IV, IVa	IV, IVa	IV, VII

It is clear from table 3 that the introduction of anisotropic vibrations in model Ia decreases the value of R_w at all temperatures. At temperatures above 873 K, an

Table 4. Parameter values of the models which give the best fit to the data at each temperature. The fitted parameter values from model IV are also given for the temperatures 1123, 1273 and 1603 K. The symbol * denotes a fixed value and the error in the last digit is given in parentheses.

	Temperature (K)												
	293	873	873	1123	1123	1273	1273	1373	1373	1473	1473	1603	1603
Model	Ia	Ia	Ia	II	IV	VI	IV	IV	IVa	IV	IVa	IV	VII
S	99*	133*	133*	129*	129*	127*	127*	125*	125*	123*	123*	121*	121*
e	0.063(3)	0.120(4)	0.056(3)	0.049(4)	0.050(4)	0.125(6)	0.122(6)	0.117(8)	0.117(8)	0.15(1)	0.15(1)	0.17(2)	0.17(2)
B_{Li} (Å^2)	0.74(2)	2.43(3)	2.34(3)	3.29(5)	3.33(4)	4.0(1)	4.24(7)	5.0(1)	5.1(1)	5.7(1)	5.8(2)	6.3(2)	5.8(3)
B_O (Å^2)	0.40(1)	1.43(1)	1.36(1)	1.91(1)	1.91(1)	2.45(1)	2.45(2)	2.74(2)	2.74(2)	3.19(2)	3.19(2)	3.84(3)	3.85(3)
$^{AN}B_{Li} \times 10^3$	−0.4(3)	−3.0(5)	−2.6(4)	−4.8(7)	−4.8(7)	−8.1(9)	−8.5(9)	−13.(2)	−14.(2)	−16.(2)	−16.(2)	−23.(4)	−23.*
B_{ILi} (Å^2)	—	—	—	—	(= B_{Li})	(= B_{Li})	(= B_{Li})	(= B_{Li})	3.(1)	(= B_{Li})	4.(1)	(= B_{Li})	(= B_{Li})
B_{RLi} (Å^2)	—	—	—	—	—	—	—	—	—	—	—	—	(= B_{Li})
n_d	0.0*	0.0*	0.0*	0.04(2)	0.02(1)	0.11(4)	0.03(1)	0.05(1)	0.04(2)	0.09(2)	0.07(2)	0.17(3)	0.46(9)
d_x	—	—	—	—	0.0*	0.0*	0.0*	0.0*	0.0*	0.0*	0.0*	0.0*	0.67*
x	—	—	—	—	—	—	—	—	—	—	—	—	0.286(7)
y	—	—	—	—	0.0*	0.17(1)	0.0*	0.0*	0.0*	0.0*	0.0*	0.0*	0.02(3)

improvement in the fits is achieved by adopting model II and allowing vacancies to form on the cation sublattice. The assumption in model II, that the time-averaged positions of the displaced cations are random, is physically unrealistic but gives firm evidence for the onset of thermally induced lithium ion disorder in Li_2O. At temperatures higher than 1123 K, significantly better fits are obtained by allowing displaced cations to occupy either I or R sites. It is important to note that no improvement in fit over model Ia is achieved by restricting the displaced cations to the empty cube-centre sites in model III.

Very good fits to all the high temperature data are obtained using model IV, constraining the displaced cations to occupy cube-edge, I sites, with $y = 0$. In model IVa, B^{I}_{Li} is allowed to vary independently from B_{Li} resulting in values, when the fit did not diverge, that are close to B_{Li}. This justifies constraining $B^{I}_{Li} = B_{Li}$ in other models, in order to reduce the number of fitted parameters. Allowing the interstitials to move off the cube-edge site in model VI only improves the fit at 1273 K, giving $y = 0.17(1)$. Model V does not fit the high temperature data as well as model IV, but is significantly better than model II and VI, suggesting that the R sites as well as I sites may be populated at high temperatures.

Only at the highest temperature does the cluster model (VII) fit the data marginally better than model IV, giving $y = 0.02(3)$, $x = 0.31(1)$ and $n_d = 0.46(9)$. From equation (11), this gives $n_f = 0.15(3)$, which is consistent with the value of 0.17(3) obtained from model IV. There is no significant improvement to the fit at this temperature by using model VIII, which gives an optimum value of the variable $d_x = 0.7(3)$ at 1603 K.

The results from model VII suggest that the time-averaged position of the lithium ion Frenkel interstitials is virtually on the cube-edge at the highest temperatures and that some adjacent regular site lithium ions relax a small distance in a (111) direction off their regular sites towards empty cube-centres. It is possible that these relaxations are related to the anharmonic thermal vibrations of these regular site ions, and not to the presence of the adjacent lithium interstitial. Overall, it would seem that the simplest model which best fits the high temperature data is model IV. Consequently, best-fit parameter values using this model are included in table 4 for the temperatures 1123, 1273 and 1603 K.

The variation of the lithium Frenkel interstitial concentration, n_f, obtained using model IV is given as a function of temperature in figure 2. The harmonic and anharmonic thermal parameters, B_{Li}, B_O and $^{AN}B_{Li}$, are given as functions of temperature in figures 3 and 4, using values given by model Ia for temperatures up to 873 K and model IV for higher temperatures. The single particle potential parameters, α_{Li}, β_{Li} and α_O, have been determined using equations (7) and (9) and are displayed graphically in figure 5.

5. Discussion

Figure 2 clearly shows that there is a rapid increase in n_f, the fraction of lithium ions leaving their regular sites to form Frenkel interstitials, with increasing temperature. The onset of this disorder, and hence the fast-ion transition temeprature T_c, can be estimated to be in the region of 1200 K ($0.7\,T_m$). At 1603 K the values of n_f determined using models IV and VII are in good agreement, from which we may conclude, with confidence, that n_f is close to 0.16 at this temperature.

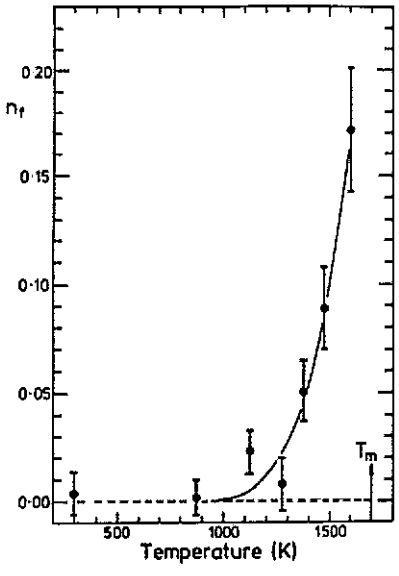

Figure 2. Temperature variation of the fraction of lithium ions, n_f, that leave their regular sites to occupy Frenkel interstitial positions (I sites) in the Li_2O lattice. The values are those that best fit the data at each temperature using the model IV (see text). The line represents the best fit to the data for n_f of the exponential function given in equation (14).

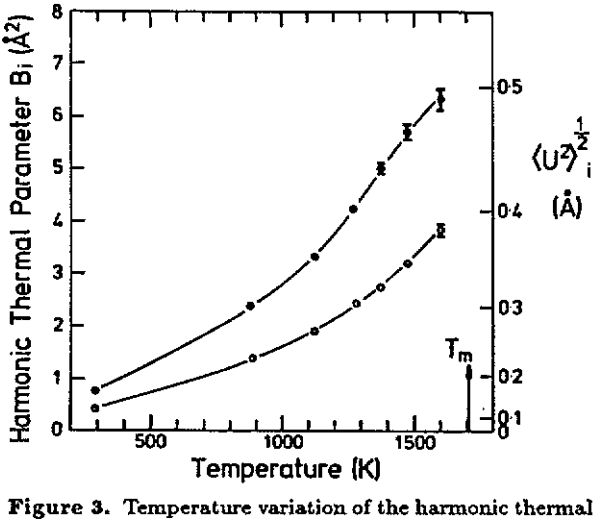

Figure 3. Temperature variation of the harmonic thermal vibration parameters for lithium, B_{Li} (●), and oxygen, B_O (○), ions in Li_2O.The root-mean-square thermal displacement of the ions may also be determined from this graph. The lines are guides to the eye.

An estimate of the Frenkel pair formation energy, E_f, for Li_2O has been obtained by fitting the experimental values for n_f given by model IV to the function

$$n_f = n_0 \exp -(E_f/2k_BT) \tag{14}$$

where n_0 is a constant. The resulting value of $E_f = 2.1(3)$ eV compares favourably with

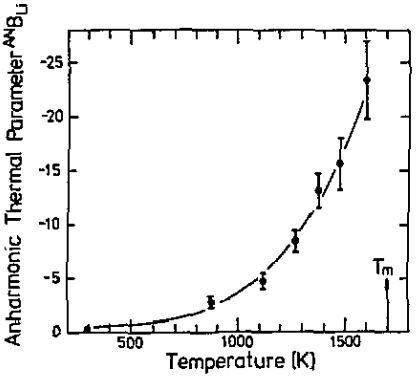

Figure 4. Temperature variation of the anharmonic thermal vibration parameter, $^{AN}B_{Li}$, for the lithium ions in Li_2O. The line is a guide to the eye.

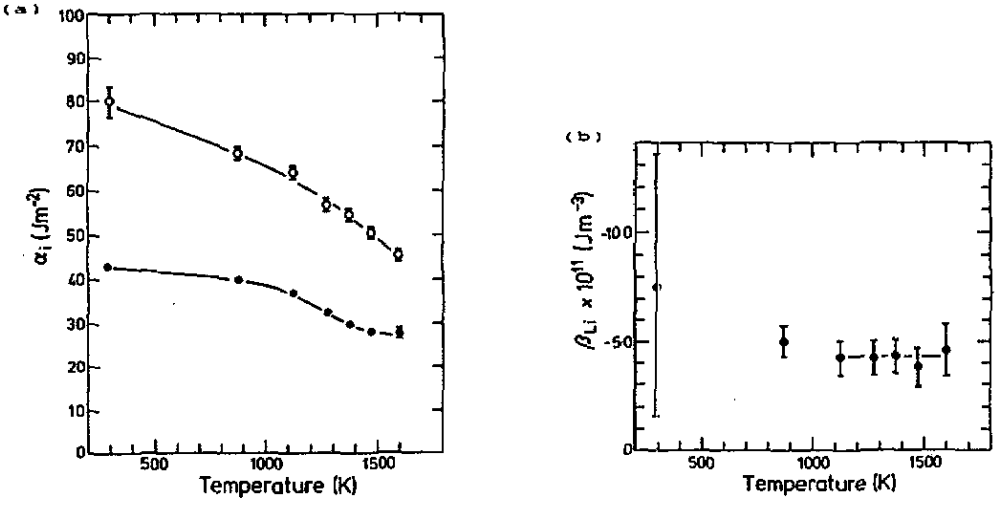

Figure 5. (*a*) Temperature variation of the harmonic one-particle potential parameters, α_{Li} (●) and α_O (○), for Li_2O. (*b*) Temperature variation of the anharmonic one-particle potential parameter, β_{Li}, for Li_2O. The lines are guides to the eye.

the reported values obtained from measurements of the ionic conductivity (2.53 eV) and from computer simulation studies (2.12 eV) (Chadwick *et al* 1988).

The onset of cation disorder is accompanied by a greater rate of increase in both a_0 and B_{Li} with increasing temperature. This anomalous behaviour is not seen, to any significant extent, in the temperature variation of B_O. The harmonic vibration root-mean-square displacement of the regular site cations $\langle u_{Li}^2 \rangle$ has been calculated using equation (8). From figure 3 it can be seen that the mean displacement $\sqrt{\langle u_{Li}^2 \rangle}$ rises with temperature to values approaching 0.5 Å near T_m. This represents a considerable fraction of the separation of the regular cation sites $\approx$ 2.4 Å ($= a_0/2$), indicating an extensive smearing of the cation positions at high temperatures. The harmonic single particle potential of Li decreases more rapidly than that of O as the temperature passes through T_c (figure 5(*a*)). The anharmonic parameter, $^{AN}B_{Li}$, increases rapidly with temperature above T_c, accounting for the increased anisotropy of larger amplitude

vibrations of regular site cations. The resulting cubic potential coefficient, β_{Li}, does not vary significantly with temperature and at temperatures above 873 K is equal to approximately -4.4×10^{11} J m^{-3}.

At the highest temperature, 1603 K, model VII suggests that the time-averaged position of the interstitial lithium ions is very close to the midpoint of the cube-edge, and that their presence is possibly the cause of the very slight ⟨111⟩ relaxation of the nearest-neighbour regular site cations towards empty cube-centre sites. Comparing the values of the positional parameters x and y with the corresponding values for the fast-ion phase of the fluorite-structured compounds, (table 5) indicates that the lithium interstitials produce considerably less distortion of the surrounding Li_2O lattice than anion Frenkel interstitials in the halide fluorites. This observation can be understood by considering the relative ionic sizes because, in the antifluorite Li_2O, it is the smaller Li^+ cation which is the disordered species at elevated temperatures.

Table 5. Comparison of the positional parameters, x and y, of ions in the 3:1:2 cluster, determined by neutron diffraction measurements.

Compound	Interstitial x position	Relaxed ion y position	Reference
Li_2O	0.29(1)	0.0	This work
CaF_2	0.33(3)	—	Hutchings *et al* (1984)
$SrCl_2$	0.38(1)	0.14(1)	Hutchings *et al* (1984)
PbF_2	0.37(1)	0.07(1)	Hutchings *et al* (1984)
UO_2	0.34	0.04	Macdonald (1985)

6. Conclusions

Single-crystal neutron diffraction measurements have been performed on $^7Li_2O$ at seven temperatures between 293 and 1603 K. The corrected, observed Bragg peak intensities have been successfully analysed using models of the time-averaged structure, with harmonic and anharmonic temperature factors to describe the mean effects of thermal vibration.

The regular fluorite structure accounts well for the observed data at temperatures up to 873 K, the data at higher temperatures can only be well fitted if a fraction of cations are allowed to leave their regular sites, creating vacancies, and occupy specific regions within the crystal lattice. Several models of the time-averaged disordered structure have been fitted to the high temperature data. There is no evidence to suggest that the empty cube-centre sites are occupied by displaced lithium ions at any temperature. In the fast-ion phase of Li_2O, mobile interstitial lithium ions occupy mean positions very close to the midpoint of the cube-edge. The fraction of lithium ions occupying these cube-edge sites increases rapidly in the region of $T \approx 1200$ K, reaching approximately 16% at 1603 K. There is also some evidence for slight ⟨111⟩ relaxations of the two nearest-neighbour regular site lithium ions towards the empty cube-centres. The parameters describing the best-fitting model to the time-averaged structure can be used to calculate the mean cation probability density function of the unit cell.

The results presented in this paper support the existence of a disordered fast-ion phase within Li_2O suggested by measurements of the self-diffusion coefficients of Li_2O by Oishi *et al* (1979) and Akiyama *et al* (1981). The transition temperature is estimated as $T_c = 1200$ K and the formation energy for the Li^+ Frenkel defects is estimated to be $E_f = 2.1(3)$ eV. Further information concerning the diffusion rate and hopping geometry have recently been provided by measurements of the quasi-elastic broadening of the diffuse incoherent neutron scattering from single crystals of $^7Li_2O$. These indicate that the majority of hops occur between nearest-neighbour sites in ⟨001⟩ directions and will be discussed in a future publication (Farley *et al* 1990).

Acknowledgments

We are grateful to R C C Ward of the Clarendon Laboratory for growing the single crystal sample used in the work presented in this paper and to M J Cooper and B T M Willis for helpful discussions concerning the TDS corrections to the diffraction data. TWDF wishes to acknowledge support from an SERC CASE award and SH support from a Harwell EMR contract. This work was undertaken as part of the underlying research programme of the United Kingdom Atomic Energy Authority.

Appendix 1

The structure factor for a unit cell of Li_2O may be expressed as a product of the structure factor for the four face-centred cubic lattice points and that for the basis of the lithium and oxygen ions.

$$F(hkl) = [1 + \cos\pi(h+k) + \cos\pi(k+l) + \cos\pi(l+h)].[b_O e^{-W_O} + b_{Li}F_i]$$

where F_i is the contribution from the lithium ions for model i, given as follows

$$F_I = 2\cos\pi/2(h+k+1)e^{-W_{Li}}$$

$$F_{Ia} = F_I^{AN} B_{Li}.hkl$$

$$F_{II} = (1-n_d)F_{Ia}$$

$$F_{III} = F_{II} + n_d e^{-W_{RLi}}F_R \qquad \text{with } x = 0.5 \text{ and } W_{RLi} = W_{Li}$$

$$F_{IV} = F_{II} + n_d e^{-W_{ILi}}F_I \qquad \text{with } y = 0.0 \text{ and } W_{ILi} = W_{Li}$$

$$F_{IVa} = F_{II} + n_d e^{-W_{ILi}}F_I$$

$$F_V = F_{II} + n_d e^{-W_{RLi}}F_R \qquad \text{with } W_{RLi} = W_{Li}$$

$$F_{VI} = F_{II} + n_d e^{-W_{ILi}}F_I \qquad \text{with } W_{ILi} = W_{Li}$$

$$F_{VII} = F_{II} + n_d(\tfrac{2}{3}e^{-W_{RLi}}F_R + \tfrac{1}{3}e^{-W_{ILi}}F_I) \qquad \text{with } W_{RLi} = W_{ILi} = W_{Li}$$

$$F_{VIII} = F_{II} + n_d(d_x e^{-W_{RLi}}F_R + [1-d_x]e^{-W_{ILi}}F_I) \qquad \text{with } W_{RLi} = W_{ILi} = W_{Li}$$

where

$$W_{Li} = B_{Li}(\sin\theta_{hkl}/\lambda)^2$$

$$W_O = B_O(\sin\theta_{hkl}/\lambda)^2$$

$$F_I = \tfrac{1}{3}\cos\pi(h+k+l)[\cos m(h+k) + \cos m(k+l) + \cos m(l+h) + \cos m(h-k) + \cos m(k-l) + \cos m(l-h)]$$

$$F_R = \tfrac{1}{2}[\cos 2\pi x(h+k+l) + \cos 2\pi x(h+k-l) + \cos 2\pi x(h-k+l) + \cos 2\pi x(k+l-h)]$$

and

$$m = \pi(1-4y)/2.$$

Appendix 2

This appendix gives the observed Bragg intensities, I_o, and the error in each intensity ΔI_o. The thermal diffuse scattering correction factor, α, has been calculated from the theory of slower than sound neutrons and is listed for each reflection. The calculated intensities, I_c, are given for the model which best fits the observed data at each temperature.

$h\ k\ l$	α	I_o	ΔI_o	I_c	$I_o - I_c$
T = 293 K				Model Ia	
0 2 2	0.0011	64.8	4.8	66.5	−1.7
1 1 3	0.0013	569.6	15.3	547.6	22.1
1 3 3	0.0028	446.7	13.6	446.0	0.7
0 2 4	0.0032	829.8	19.4	841.1	−11.3
2 2 4	0.0036	49.2	3.6	49.5	−0.3
3 3 3	0.0044	387.9	11.9	377.3	10.6
1 1 5	0.0046	371.5	11.6	382.3	−10.8
0 4 4	0.0056	47.7	3.7	47.7	0.0
1 3 5	0.0069	348.5	11.7	336.2	12.3
2 4 4	0.0064	651.3	15.0	683.6	−32.3
0 2 6	0.0072	49.3	3.6	47.0	2.3
3 3 5	0.0074	308.0	10.1	311.3	−3.3
2 2 6	0.0085	655.7	15.5	627.8	27.9
4 4 4	0.0074	36.3	2.6	47.0	−10.7
1 5 5	0.0078	288.9	9.7	283.8	5.1
1 1 7	0.0082	271.3	9.7	280.3	−9.0
0 4 6	0.0095	596.6	14.5	581.1	15.6
2 4 6	0.0080	48.2	2.7	47.5	0.7
3 5 5	0.0094	254.2	9.1	254.8	−0.6
1 3 7	0.0096	269.7	9.7	264.8	4.9
4 4 6	0.0108	516.7	12.8	512.7	4.0
0 2 8	0.0126	501.3	13.4	514.0	−12.7
2 2 8	0.0127	60.1	4.3	50.5	9.6
5 5 5	0.0153	245.1	9.7	252.7	−7.6
1 5 7	0.0126	248.8	9.5	237.3	11.5
2 6 6	0.0149	495.0	14.0	493.3	1.7
0 4 8	0.0167	63.1	4.6	53.3	9.8

$h\ k\ l$	α	I_o	ΔI_o	I_c	$I_o - I_c$
1 1 9	0.0219	229.6	7.8	239.9	−10.3
3 5 7	0.0170	267.2	10.7	247.0	20.2
2 4 8	0.0221	477.9	15.4	485.2	−7.3
1 3 9	0.0275	228.5	11.4	241.4	−12.9
T = 873 K (first run)				Model Ia	
0 2 2	0.0037	90.4	5.2	97.6	−7.2
1 1 3	0.0046	498.6	18.5	495.0	3.6
1 3 3	0.0101	373.3	15.0	378.9	−5.6
0 2 4	0.0114	651.3	20.5	628.6	22.7
2 2 4	0.0129	76.2	4.5	71.0	5.3
3 3 3	0.0157	260.4	12.1	261.6	−1.2
0 4 4	0.0200	60.6	3.7	62.9	−2.3
1 3 5	0.0247	214.4	10.6	208.0	6.4
2 4 4	0.0228	363.7	13.1	388.8	−25.1
0 2 6	0.0258	56.8	3.7	55.5	1.3
3 3 5	0.0264	186.9	9.9	184.6	2.3
4 4 4	0.0296	47.0	2.9	48.6	−1.6
1 5 5	0.0282	135.9	7.5	136.4	−0.5
2 4 6	0.0293	41.3	2.7	42.2	−0.9
3 5 5	0.0343	87.4	5.8	85.6	1.8
1 3 7	0.0351	112.1	7.2	106.1	6.0
4 4 6	0.0396	139.4	7.9	135.8	3.6
0 2 8	0.0462	134.5	7.7	136.8	−2.3
5 5 5	0.0620	86.6	6.4	82.0	4.6
2 6 6	0.0548	103.8	6.6	107.2	−3.4
3 5 7	0.0630	60.8	4.7	63.9	−3.1
2 4 8	0.0807	88.4	5.0	86.9	1.5
4 6 6	0.0828	26.9	2.0	26.0	0.9
T = 873 K (second run)				Model Ia	
0 2 2	0.0040	105.9	6.1	102.0	4.0
1 1 3	0.0051	666.5	15.0	653.8	12.7
1 3 3	0.0112	460.9	11.9	466.8	−5.9
0 2 4	0.0126	878.9	17.9	888.9	−10.0
2 2 4	0.0142	75.9	4.2	74.2	1.7
3 3 3	0.0173	306.1	9.5	310.2	−4.1
1 1 5	0.0179	349.4	10.2	336.8	12.6
0 4 4	0.0220	68.9	4.1	66.2	2.7
1 3 5	0.0272	252.3	8.7	241.1	11.2
2 4 4	0.0251	473.8	11.3	491.4	−17.6
0 2 6	0.0284	60.4	3.7	58.8	1.6
3 3 5	0.0290	202.8	6.9	209.3	−6.5
2 2 6	0.0334	375.0	10.6	367.7	7.3
4 4 4	0.0326	49.2	3.2	51.9	−2.7
1 5 5	0.0310	159.9	6.4	154.3	5.6
1 1 7	0.0359	150.7	6.1	145.2	5.5
0 4 6	0.0376	302.3	9.2	275.9	26.4
2 4 6	0.0323	44.3	3.1	45.5	−1.2
3 5 5	0.0377	94.1	4.8	99.2	−5.1
1 3 7	0.0386	117.0	5.2	120.1	−3.1
4 4 6	0.0436	162.9	6.2	160.2	2.7
0 2 8	0.0559	152.2	6.4	162.2	−10.0
2 2 8	0.0513	34.5	2.5	35.7	−1.2
5 5 5	0.0681	90.5	5.1	92.1	−1.6

h k l	α	I_o	ΔI_o	I_c	$I_o - I_c$
1 5 7	0.0513	74.7	4.4	70.4	4.3
2 6 6	0.0602	124.1	6.0	126.6	−2.5
0 4 8	0.0744	31.2	2.5	32.3	−1.1
1 1 9	0.0878	64.1	4.5	64.3	−0.2
3 5 7	0.0692	75.6	4.8	72.6	3.0
2 4 8	0.0886	99.3	6.0	103.2	−3.9
1 3 9	0.1112	51.4	4.3	52.7	−1.3
$T = 1123$ K				Model II	
0 2 2	0.0054	119.2	5.3	123.7	−4.5
1 1 3	0.0071	597.8	16.3	594.1	3.8
1 3 3	0.0155	393.6	12.9	392.4	1.2
0 2 4	0.0174	701.4	17.5	719.2	−17.8
2 2 4	0.0196	87.7	4.0	77.5	10.2
3 3 3	0.0239	222.3	9.2	220.8	1.5
1 1 5	0.0247	256.4	7.1	253.8	2.6
0 4 4	0.0304	63.3	3.2	63.0	0.3
1 3 5	0.0376	170.6	8.1	159.5	11.2
2 4 4	0.0347	307.5	10.3	306.1	1.4
0 2 6	0.0393	50.4	1.9	50.7	−0.3
3 3 5	0.0402	137.3	6.6	134.6	2.7
2 2 6	0.0462	209.9	6.4	202.5	7.4
4 4 4	0.0451	40.0	1.8	40.3	−3.0
1 5 5	0.0430	84.6	4.7	87.3	−2.7
1 1 7	0.0498	84.0	3.7	79.7	4.3
0 4 6	0.0522	148.4	5.3	134.9	13.5
2 4 6	0.0448	30.7	1.9	31.7	−1.0
3 5 5	0.0523	46.5	3.4	46.4	0.1
1 3 7	0.0536	62.5	3.1	61.1	1.4
4 4 6	0.0607	62.7	3.0	62.6	0.2
0 2 8	0.0778	59.5	3.0	63.6	−4.1
2 2 8	0.0714	19.3	1.5	20.0	−0.7
5 5 5	0.0949	38.8	2.3	40.4	−1.6
1 5 7	0.0715	26.0	1.7	28.4	−2.4
2 6 6	0.0926	44.7	2.5	45.0	−0.3
0 4 8	0.1038	16.1	1.2	16.3	−0.2
1 1 9	0.1226	21.9	1.4	24.3	−2.4
3 5 7	0.1067	30.3	1.7	28.5	1.8
2 4 8	0.1237	30.9	1.8	33.0	−2.1
1 3 9	0.1544	18.4	1.7	17.8	0.6
$T = 1273$ K				Model VI	
0 2 2	0.0066	112.6	5.1	115.2	−2.6
1 1 3	0.0087	422.8	10.3	418.0	4.8
1 3 3	0.0191	271.1	10.5	282.0	−10.9
0 2 4	0.0215	441.2	14.4	434.0	7.2
2 2 4	0.0242	74.4	3.6	70.0	4.4
3 3 3	0.0294	131.4	6.3	143.8	−12.4
0 4 4	0.0374	50.1	2.8	52.8	−2.7
1 3 5	0.0463	107.1	6.3	98.9	8.2
2 4 4	0.0427	173.8	8.1	179.7	−5.9
0 2 6	0.0484	40.5	1.9	38.9	1.6
3 3 5	0.0495	88.2	5.1	85.9	2.3
4 4 4	0.0557	26.5	1.3	26.6	−0.1
1 5 5	0.0585	47.8	3.1	49.6	−1.8

$h\ k\ l$	α	I_o	ΔI_o	I_c	$I_o - I_c$
2 4 6	0.0552	18.9	1.1	19.4	−0.5
3 5 5	0.0643	22.5	2.0	21.6	0.9
1 3 7	0.0729	30.7	2.6	31.7	−1.0
4 4 6	0.0749	29.0	1.9	26.7	2.3
0 2 8	0.0961	27.6	2.4	27.8	−0.2
5 5 5	0.1174	18.2	1.5	19.5	−1.3
2 6 6	0.1146	19.4	1.6	17.9	1.5
3 5 7	0.1323	12.2	1.1	12.1	0.1
2 4 8	0.1533	12.1	0.9	12.1	0.0
4 6 6	0.1583	5.3	0.6	5.3	0.0
$T = 1373$ K				Model IV	
0 2 2	0.0093	130.3	5.6	135.3	−5.0
1 1 3	0.0125	390.9	13.9	392.6	−1.7
1 3 3	0.0274	271.9	10.3	266.9	5.0
0 2 4	0.0309	396.8	13.1	399.9	−3.1
2 2 4	0.0346	79.7	4.0	73.9	5.9
3 3 3	0.0421	113.7	6.2	116.1	−2.4
0 4 4	0.0534	46.1	2.8	49.7	−3.6
1 3 5	0.0652	90.8	5.8	81.4	9.4
2 4 4	0.0609	142.3	6.9	137.8	4.6
0 2 6	0.0689	42.6	2.1	37.2	5.4
3 3 5	0.0706	71.2	4.6	71.7	−0.5
4 4 4	0.0793	24.1	1.4	24.5	−0.4
1 5 5	0.0834	35.5	2.8	38.6	−3.1
2 4 6	0.0808	16.0	1.1	17.1	−1.1
3 5 5	0.0940	13.9	1.4	14.8	−0.9
1 3 7	0.1040	24.1	2.2	23.3	0.8
4 4 6	0.1095	16.6	1.3	16.2	0.4
0 2 8	0.1363	17.7	1.8	16.6	1.1
5 5 5	0.1620	12.1	1.2	12.4	−0.3
2 6 6	0.1604	10.6	1.0	10.1	0.5
3 5 7	0.1820	7.1	0.8	7.3	−0.2
2 4 8	0.1953	6.3	0.6	6.6	−0.3
4 6 6	0.2045	3.5	0.4	3.8	−0.3
$T = 1473$ K				Model IV	
0 2 2	0.0101	139.3	5.6	141.3	−2.0
1 1 3	0.0136	323.6	11.5	335.2	−11.6
1 3 3	0.0296	232.2	9.9	222.8	9.4
0 2 4	0.0334	326.7	11.9	317.9	8.8
2 2 4	0.0374	69.3	3.6	68.2	1.1
3 3 3	0.0455	86.1	5.2	87.9	−1.8
0 4 4	0.0578	34.6	2.3	38.2	−3.6
1 3 5	0.0707	61.5	4.4	58.8	2.7
2 4 4	0.0658	98.0	5.9	95.8	2.2
0 2 6	0.0745	33.8	1.7	29.4	4.4
3 3 5	0.0764	48.6	3.8	49.3	−0.7
4 4 4	0.0859	17.7	1.2	16.0	1.7
1 5 5	0.0904	26.6	2.5	24.4	2.2
2 4 6	0.0863	10.1	0.7	11.4	−1.3
3 5 5	0.1100	8.8	0.9	8.8	0.0
1 3 7	0.1127	12.1	1.1	13.7	−1.6
4 4 6	0.1171	8.6	0.8	8.5	0.2
0 2 8	0.1481	8.2	0.7	8.7	−0.5

h k l	α	I_o	ΔI_o	I_c	$I_o - I_c$
5 5 5	0.1766	5.7	0.5	6.2	−0.5
2 6 6	0.1747	4.9	0.5	4.6	0.3
3 5 7	0.1986	3.6	0.4	3.4	0.2
2 4 8	0.2135	3.2	0.3	3.0	0.2
4 6 6	0.2236	1.8	0.2	1.9	−0.1
$T = 1603$ K				Model VII	
0 2 2	0.0155	153.2	6.3	156.4	−3.2
1 1 3	0.0215	285.4	10.8	287.0	−1.6
1 3 3	0.0433	180.2	8.6	181.5	−1.3
0 2 4	0.0471	253.2	10.9	246.0	7.2
2 2 4	0.0560	61.7	3.5	55.8	5.9
3 3 3	0.0661	57.2	4.4	58.8	−1.6
1 1 5	0.0671	92.5	4.4	89.6	2.9
0 4 4	0.0822	26.0	2.0	27.1	−1.1
1 3 5	0.0955	36.7	3.2	36.1	0.6
2 4 4	0.0940	53.8	4.0	60.3	−6.5
0 2 6	0.1063	21.3	1.4	19.0	2.3
3 3 5	0.1120	25.9	2.4	31.7	−5.8
2 2 6	0.1218	27.5	1.9	26.3	1.2
4 4 4	0.1263	9.4	0.7	9.1	0.3
1 5 5	0.1338	12.6	1.4	13.7	−1.1
1 1 7	0.1375	9.3	1.0	10.6	−1.3
0 4 6	0.1424	14.5	1.4	14.0	0.5
2 4 6	0.1322	4.3	0.5	5.6	−1.3
3 5 5	0.1605	3.0	0.3	3.3	−0.3
1 3 7	0.1628	6.6	0.6	6.8	−0.2
4 4 6	0.1875	3.3	0.4	3.6	−0.3
0 2 8	0.2035	4.2	0.4	3.5	0.7
5 5 5	0.2384	2.4	0.3	2.9	−0.5
2 6 6	0.2374	2.2	0.2	1.8	0.4
1 1 9	0.2874	0.9	0.1	1.0	−0.1
3 5 7	0.2691	1.7	0.2	1.4	0.3
2 4 8	0.2910	1.3	0.1	1.0	0.3

References

Akiyama M, Ando K and Oishi Y 1981 *Solid State Ion.* **3/4** 469

Catlow C R A and Hayes W 1982 *J. Phys. C: Solid State Phys.* **15** L9

Chadwick A V, Flack K W, Strange J H and Harding J 1988 *Solid State Ion.* **28–30** 185

Cooper M J 1971 *Acta Crystallogr.* A **27** 148

Cooper M J and Rouse K D 1968 *Acta Crystallogr.* A **24** 405

Dawson B, Hurley A C and Maslen V W 1967 *Proc. R. Soc.* A **298** 289

Dickens M H, Hayes W, Hutchings M T and Smith C 1982 *J. Phys. C: Solid State Phys.* **15** 4043

Farley T W D 1989 *DPhil Thesis* Clarendon Laboratory, University of Oxford

Farley T W D, Hayes W, Hutchings M T and Hull S 1990 to be published

Forsyth J B, Wilson C C and Sabine T M 1989 *Acta Crystallogr.* A **45** 244

Hamilton W C 1965 *Acta Crystallogr.* **18** 502

Harries D R, Dupouy J M and Wu C H 1985 *J. Nucl. Mater.* **133–4** 25

Hayes W and Hutchings M T 1989 *Ionic Solids at High Temperatures* ed A M Stoneham (Singapore: World Scientific)

Hull S, Farley T W D, Hayes W and Hutchings M T 1988 *J. Nucl. Mater.* **160** 125

Hutchings M T, Clausen K N, Dickens M H, Hayes W, Kjems J K, Schnabel P G and Smith C 1984 *J. Phys. C: Solid State Phys.* **17** 3903
Johnson C E, Kummerer K R and Roth E 1988 *J. Nucl. Mater.* **155–7** 188
Kulcinski G L, Dupouy J M and Ishino E 1986 *J. Nucl. Mater.* **141–3** 3
Larson A C 1967 *Acta Crystallogr.* **23** 664
Liu Y Y, Billone M C, Fischer A K, Tam S W and Clemmer R G 1985 *J. Fusion Technol.* **8** 1970
Macdonald J E 1985 *DPhil Thesis* Clarendon Laboratory, University of Oxford
Ohno H, Konishi S, Nagasaki T, Kurasawa T, Katsuta H and Watanabe H 1985 *J. Nucl. Mater.* **133–4** 181
Oishi Y, Kamei Y, Akiyama M and Yanagi T 1979 *J. Nucl. Mater.* **87** 341
Smith D L, Baker C C, Sze D K, Morgan G D, Abdou M A, Piet S J, Schultz K R, Moir R W and Gorden J D 1985 *Fusion Technol.* **8** 9
Willis B T M 1965 *Acta Crystallogr.* **18** 75
—— 1970 *Acta Crystallogr.* A **26** 396
Willis B T M and Hazell R G 1980 *Acta Crystallogr.* A **36** 582
Zachariasen W H 1967 *Acta Crystallogr.* **23** 558